Unraveling bulk and grain boundary electrical properties in $La_{0.8}Sr_{0.2}Mn_{1-y}O_{3\pm\delta}$ thin films

Francesco Chiabrera, Iñigo Garbayo, Dolors Pla, Mónica Burriel, Fabrice Wilhelm, Andrei Rogalev, Marc Núñez, Alex Morata, and Albert Tarancón

Unraveling bulk and grain boundary electrical properties in La$_{0.8}$Sr$_{0.2}$Mn$_{1-y}$O$_{3\pm\delta}$ thin films

View Online   Export Citation   CrossMark

Francesco Chiabrera,[1] [iD] Iñigo Garbayo,[1] [iD] Dolors Pla,[2] Mónica Burriel,[2] Fabrice Wilhelm,[3] Andrei Rogalev,[3] Marc Núñez,[1] Alex Morata,[1] and Albert Tarancón[1,4,a)]

AFFILIATIONS

[1] Department of Advanced Materials for Energy, Catalonia Institute for Energy Research (IREC), Jardí de les Dones de Negre 1, Planta 2, 08930 Sant Adrià de Besòs, Barcelona, Spain
[2] Univ. Grenoble Alpes, CNRS, Grenoble INP (Institute of Engineering Univ. Grenoble Alpes), LMGP, F-38000 Grenoble, France
[3] European Synchrotron Radiation Facility (ESRF), F-38054 Grenoble, France
[4] ICREA, Passeig Lluís Companys 23, 08010 Barcelona, Spain

[a)] Author to whom correspondence should be addressed: atarancon@irec.cat

ABSTRACT

Grain boundaries in Sr-doped LaMnO$_{3\pm\delta}$ thin films have been shown to strongly influence the electronic and oxygen mass transport properties, being able to profoundly modify the nature of the material. The unique behavior of the grain boundaries can be correlated with substantial modifications of the cation concentration at the interfaces, which can be tuned by changing the overall cationic ratio in the films. In this work, we study the electronic properties of La$_{0.8}$Sr$_{0.2}$Mn$_{1-y}$O$_{3\pm\delta}$ thin films with variable Mn content. The influence of the cationic composition on the grain boundary and grain bulk electronic properties is elucidated by studying the manganese valence state evolution using spectroscopy techniques and by confronting the electronic properties of epitaxial and polycrystalline films. Substantial differences in the electronic conduction mechanism are found in the presence of grain boundaries and depending on the manganese content. Moreover, the unique defect chemistry of the nanomaterial is elucidated by measuring the electrical resistance of the thin films as a function of oxygen partial pressure, disclosing the importance of the cationic local non-stoichiometry on the thin film behavior.

Engineering the transport properties of complex oxides is considered one of the major challenges for launching the next generation of highly performing solid state devices. In this direction, mastering the implementation of interface-dominated materials represents a powerful engineering tool with implications in many different fields. For instance, grain boundaries (GBs) and dislocations have been demonstrated to substantially increase oxygen diffusion in La$_{0.8}$Sr$_{0.2}$MnO$_{3\pm\delta}$ (LSM) thin films, improving their performance as cathodes in solid oxide fuel cells.[1-4] On the other hand, GBs are also responsible for a strong reduction of magnetic order and electronic structure in manganites, which can be used in

spintronics and resistive switching devices.[5,6] In this sense, GBs are generally considered as an insulating paramagnetic region, whose presence can give rise to a collection of unique properties, such as a large magnetoresistance below the Curie temperature[7,8] or the appearance of different low temperature conduction mechanisms in polycrystalline thin films.[9,10]

We recently showed that the GBs in LSM thin films are dominated by an unusual local modification of chemical composition, which involves both the oxygen and the cations.[11] Moreover, we demonstrated that this local non-stoichiometry is modifiable by simply changing the overall cationic ratio

Mn/(La+Sr) in the thin films. This way, for highly Mn deficient thin films, the GBs (GB$_{def}$) are characterized by additional depletion of Mn and O, while La and Sr increase. When the overall Mn concentration rises (GB$_{rich}$), the interfaces completely change the cationic distribution, turning to La (and O) deficient regions with a progressive increase of Mn. Notably, we confirmed that the variations observed in the GB composition are the cause of strong changes in the electrical and electrochemical behavior, thus offering a powerful tool for tuning the functional properties of thin films.

In this work, we delve into the electronic conduction mechanism of La$_{0.8}$Sr$_{0.2}$Mn$_{1-y}$O$_{3\pm\delta}$ (LSM$_y$) thin films by studying, first, the impact of the different Mn/(La+Sr) ratios on the bulk behavior by spectroscopy techniques and, second, the GB properties in polycrystalline samples by confronting them with epitaxial LSM$_y$ with variable Mn content. The first analysis on the bulk defect chemistry is particularly important since large Mn deficiencies are explored in this study. In this sense, it is well-known that a change in the B/A ratio creates negative cation vacancies in LSM (V$'''_{Mn}$ or V$'''_{La}$) that need to be compensated by positive defects (V$^{\cdot\cdot}_{O}$ and/or Mn^{4+}), strongly affecting the electronic conduction properties. Using this first analysis for defining the bulk references, we aim to identify then the distinct conduction mechanism occurring at the GBs, stressing the importance of these interfaces in the overall functional properties of thin films. Finally, we discuss the impact of the specific local non-stoichiometry at the GBs on the electronic mechanism, showing the central role of Mn in defining the interface properties.

LSM$_y$ thin films with variable Mn content were deposited by combinatorial Pulsed Laser Deposition (c-PLD) on 5 mm × 10 mm sapphire (0001) substrates and on 100 nm YSZ/Si 4 in. wafers in a large-area system from PVD Products (PLD-5000), equipped with a KrF-248 nm excimer laser from Lambda Physik (COMPex PRO 205). c-PLD is a technique based on the alternate deposition of two different parent compounds (in our case La$_{0.8}$Sr$_{0.2}$MnO$_3$ and Mn$_3$O$_4$ commercial targets) at two opposite sides of a large area substrate.[12–15] Due to the typical Gaussian shape of the PLD plasma plumes, a continuous gradient of concentration is obtained between the two plume centres. For the LSM$_y$ combinatorial deposition, the sapphire samples were pasted to a 4 in. Si wafer forming a line between the LSM and Mn$_3$O$_4$ plume centers, allowing a gradual increase in B/A = Mn/(La+Sr) ratio. The LSM$_y$/YSZ/Si sample was instead deposited at the wafer level and then cut into 1 × 0.5 cm^2 rectangular specimens for the electrical and structural characterization.[11] Deposition parameters were adapted in order to obtain fully dense films with compositions from the Mn/(La+Sr) ratio of B/A = 0.85 ± 0.02 to B/A > 1.2 ± 0.03, which was confirmed by wavelength dispersive spectroscopy and energy dispersive X-ray analysis, and thicknesses between 70 and 100 nm (see details elsewhere[11]). The B/A compositional error in the structural and electrical characterization was calculated considering the variation of the B/A ratio occurring in the portion of the combinatorial sample analyzed.[11] In order to equilibrate the oxygen

stoichiometry of the samples, all the LSM$_y$ thin films were annealed for 6 h in air at 923 K after deposition. Structural and surface characterization of the thin films was performed by X-ray Diffraction (XRD) (Bruker D8 Advance diffractometer system), by Transmission Electron Microscopy (TEM) (FEI TITAN Low Base operated at 300 kV), and by non-contact Atomic Force Microscopy (AFM, XE 100 Park System Corp.). Figure 1(a) shows the Θ-2Θ XRD of the LSM$_y$ samples revealing a single phase deposition independent of the Mn content. These measurements were performed by applying an omega offset to reduce the contribution from the single crystalline substrates. A slight (110)$_{pc}$ preferential orientation is detected in the most deficient Mn thin films, which reduces on increasing the B/A ratio and disappears for the nearly stoichiometric layer. The Mn rich samples show instead a small strengthening of the (100)$_{pc}$ orientation. Figure 1(b) shows the evolution of the lattice parameters as a function of the B/A ratio. A significant linear expansion of the unit cell is observed in the Mn deficient part, while a small shrinkage is detected increasing the Mn content (B/A > 1), as previously reported.[11] The LSM$_y$ films deposited on sapphire and YSZ/Si show comparable lattice parameters, implying that the substrate is not affecting the stress state in the polycrystalline layers. At the same time, the AFM surface and TEM cross-sectional images of a typical LSM$_y$ sample with B/A = 0.92 ± 0.02, Figs. 1(c) and 1(d), respectively, prove the characteristic columnar structure and nanocrystalline grains obtained. This columnar structure, without segregation of secondary phases, was observed in all the samples independent of the overall Mn content, with a small variation of the grain size for different B/A ratios.[11]

X-ray Absorption Near-Edge Structure (XANES) and ellipsometry were carried out on the LSM$_y$ film series in order to investigate the effect of varying the B/A ratio on the overall manganese valence. It is important to note that these two techniques are not able to separate grain and grain boundary contributions; therefore, the results described next can be unambiguously ascribed to the bulk LSM$_y$ since it represents approximately the 90 vol. % of the polycrystalline films. XANES spectra at the Mn K-edge of LSM$_y$ thin films were collected at the ESRF ID12 Synchrotron beamline (Grenoble, France) under vacuum and at T = 298 K with a nearly constant beam current of 200 mA (for additional details, see Sec. S.1. of the supplementary material). Figure 2(a) shows the Mn K-edge XANES spectra of the polycrystalline LSM$_y$ thin films for different B/A ratios. Here we focus on the absorption edge region, particularly on the white line positioned at ~6554 eV. Its position for each spectrum was extracted by calculating the inflection point energy, given by the maximum of the first derivative (see Fig. S1 of the supplementary material). This feature, which involves a transition from Mn 1s to Mn 4p states, has been demonstrated to display an energy shift depending on the Mn valence in many different compounds, including perovskites.[16,17] In particular, the K-edge energy increases almost linearly with the Mn valence in LSM, shifting approximately 1 eV per 0.27 valence change.[18,19] In our samples, no significant changes were measured in the Mn deficient films
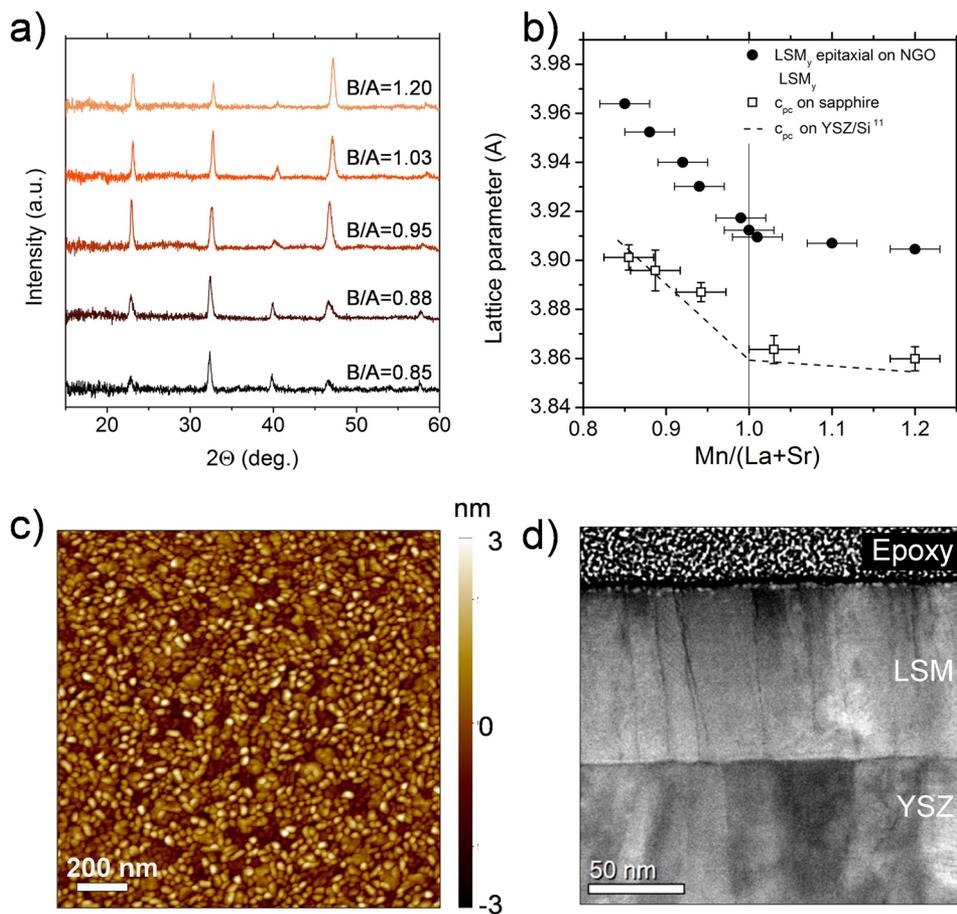
FIG. 1. (a) XRD of the polycrystalline LSM_y thin film grown on the sapphire (0001). (b) Evolution of the pseudo-cubic lattice parameter as a function of the B/A ratio derived from the XRD analysis for different substrates. (c) AFM image of the surface and (d) cross-sectional dark field TEM image of a characteristic LSM_y sample deposited on a 100 nm YSZ/Si substrate.

and only a very small increase of ~0.1 eV (corresponding to a relative increase of 3% in $[Mn^{4+}]$[18-20]) was observed in the La-rich compositions [Fig. 2(b)]. Complementary ellipsometry measurements supported the XANES results by confirming a uniform Mn valence within the Mn deficient LSM_y films (see detailed analysis in Sec. S.2. of the supplementary material). Interestingly, the optical conductivity measured shows a high sensitivity to the Mn content, offering a powerful tool to track compositional changes by studying the optical properties of the material.

According to the XANES and ellipsometry results, the bulk electro-neutrality in the Mn-deficient LSM_y films cannot be attributed to a change in the Mn valence state. The most probable compensation mechanism would be the formation of positive defects, such as oxygen vacancies, usually present in a very low concentration in stoichiometric LSM.[21,22]
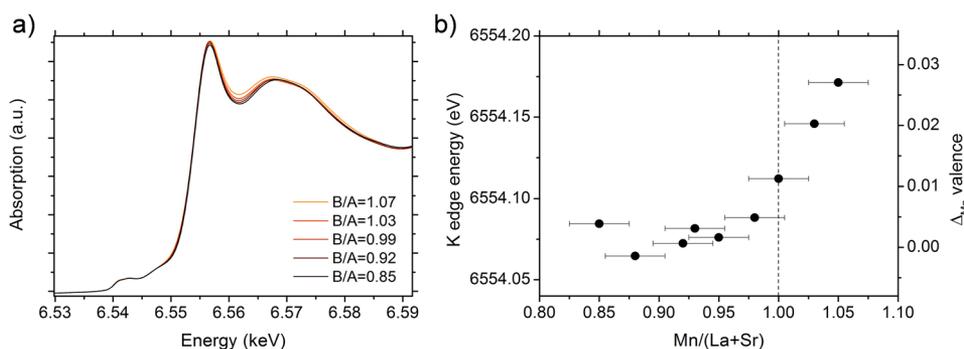
FIG. 2. (a) Normalized XANES spectra at the Mn K-edge for various B/A ratios. (b) Variation of the calculated inflection point energy with the cationic composition in LSM_y films. The corresponding relative change in Mn valence is also shown on the right axis.[18,19].

However, the total charge compensation by oxygen vacancies (with equilibrium $[V_O^{\cdot\cdot}] = 3/2 \cdot [V_{Mn}''']$) would result in a great oxygen deficiency and a much higher increase in bulk oxygen diffusion than the one observed in our previous studies.[1,3] Alternatively, we propose a different mechanism in which the cation vacancies are mainly compensated by the formation of neutral anti-site defects (La_{Mn}^x). Simple calculations after the work of Nakamura[23] (included in Sec. S.3. of supplementary material) show that this compensation mechanism radically reduces the need of oxygen vacancies to balance the charge; e.g., for the nominal composition B/A = 0.90, a concentration of La_{Mn}^x = 0.04 lowers the effective concentration of V_{Mn}''' from 0.10 to nearly 0.02 per unit-formula, implying that significantly less negative charge needs to be compensated by positive defects (i.e., oxygen vacancies). Although this mechanism is not commonly observed in bulk perovskites, similar anti-site defects have been recently reported by Qiao *et al.* in Cr deficient epitaxial $LaCrO_3$ films.[24] Moreover, recent Density Functional Theory (DFT) simulations carried out for LSM[11] showed that the formation energy of La_{Mn}^x strongly decreases in the presence of oxygen vacancies, i.e., the formation of the anti-site defects is favorable under highly reducing PLD growing conditions. This compensation mechanism is also in good agreement with the expansion of the out-of-plane lattice parameter measured in our films [see Fig. 1(b)] since the La ionic radius is significantly bigger than the Mn one. As a counterpart, for moderately Mn rich samples (B/A > 1), the presence of La vacancies (V_{La}''') can be mainly compensated by the formation of the likely occurring Mn_{La}^x anti-site defects accompanied by a small increase of Mn^{4+}, which can explain the slight shrinkage of the unit cell observed [see Fig. 1(b)].

In order to clearly identify the contribution of GBs on the electrical properties of polycrystalline LSM_y films, we compared two sets of equivalent polycrystalline [on sapphire (0001) and on YSZ/Si substrates] and epitaxial [on $NdGaO_3$ (110), NGO] samples with B/A ratios from 0.85 to 1.2. The epitaxial films showed a single phase, $(001)_{pc}$ oriented growth, with a smooth surface of rms <0.4 nm. The evolution of the out of plane lattice parameter with the B/A ratio follows the same trend of the polycrystalline layers; see Fig. 1(b) (the complete structural and compositional characterization of the epitaxial films can be found in Sec. S.4. of the supplementary material). All the samples were electrically characterized in air in a 4-point in-plane configuration by using silver electrodes in a temperature-controlled Linkam probe station, between 83 K and 873 K (in conformity with our previous studies; see Refs. 3 and 11 and Sec. S.5. of the supplementary material).

First, the in-plane electronic conductivity above room temperature of polycrystalline and epitaxial films with different Mn contents has been represented using an Arrhenius plot in Fig. 3(a). In general, the polycrystalline thin films present lower conductivity with respect to the epitaxial ones of similar composition, while an increase in conductivity is observed by increasing the Mn content, for both types of films. Independent of the composition or nature of the films, these show
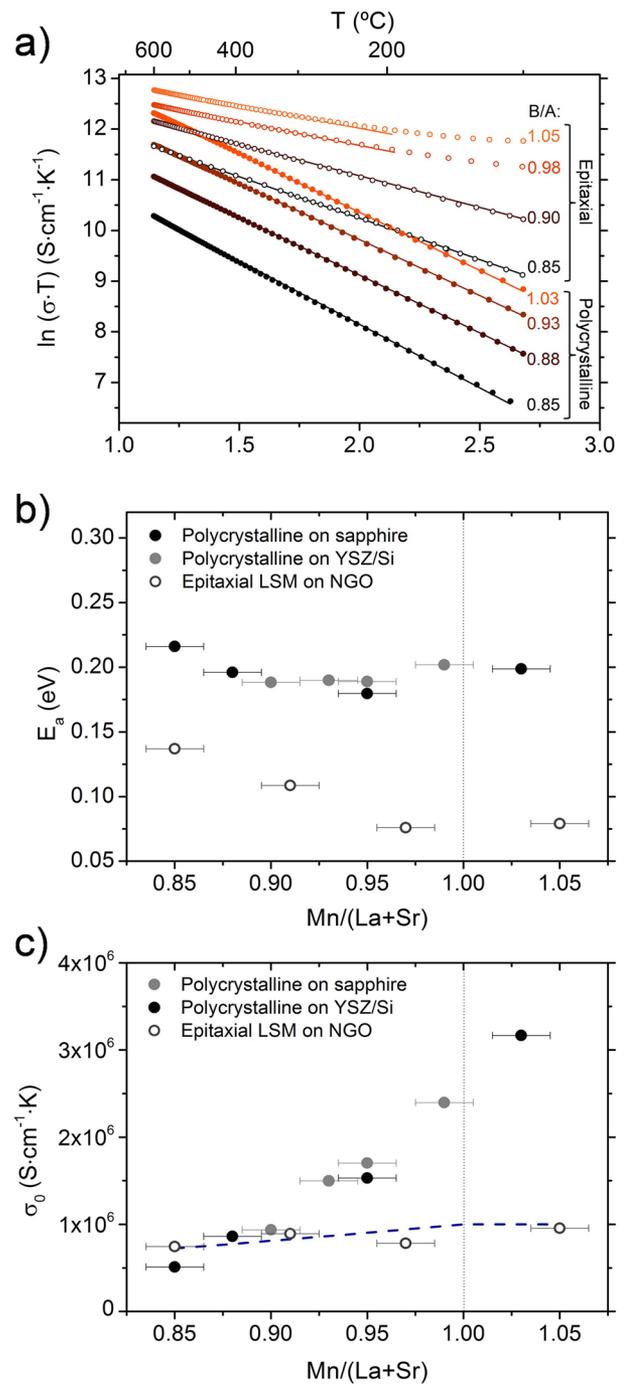
FIG. 3. (a) In-plane electronic conductivity as a function of temperature for the epitaxial and polycrystalline LSM_y thin films, plotted according to the adiabatic small polaron model. (b) Energy of activation (E_a) and (c) pre-exponential factor (σ_0) derived by the small polaron fitting. The polycrystalline samples measured on two different substrates give rise to similar results. The blue dashed line in (c) indicates the theoretical trend expected from the decrease in Mn hopping sites and no change in Mn valence ($\sigma_0 \propto [Mn]^2$).

a perfect agreement with a small polaron hopping conduction for the whole range of temperatures,[10,22,25–27] also supported by the optical measurements (see Fig. S2 of the supplementary material). According to this model, the polarons can move to the Nearest Neighbour Hopping (NNH) site with the assistance of phonons, leading to the following expression of conductivity in the case of adiabatic limit:[28]

$$\sigma(T) = \frac{\sigma_0}{T} \cdot \exp\left(\frac{E_a}{k_b T}\right), \qquad (1)$$

where E_a refers to the activation energy of the hopping mechanism, k_b is the Boltzmann constant, and σ_0 is the pre-exponential factor.

By fitting the conductivity values with Eq. (1), E_a and σ_0 have been calculated and represented in Figs. 3(b) and 3(c), respectively. First, the activation energy of the epitaxial samples is lower than that of the polycrystalline ones. Moreover, the epitaxial samples present a progressive decrease in the activation energy while increasing the B/A ratio, whereas in the polycrystalline ones E_a is kept almost constant. This can be clearly associated with the presence of structural and chemical defects in both types of GBs (GB_{def} and GB_{rich}) that cause the localization and trapping of charge carriers, breaking the conduction paths and increasing the polaron energy barrier. Noteworthy, the decrease in E_a in the epitaxial samples is consistent with the decrease observed in the out-of-plane lattice parameter [see Fig. 1(b)], which represents a reduction in the tetragonal distortion of the cell and diminishes the polaron barrier.[29–31] Also, this matches with the shift toward lower energies for both the polaron and Jahn-Teller distortion phenomena, which govern the optical transitions observed by ellipsometry when increasing the Mn content in the films (see Fig. S2 in the supplementary material).[32]

Figure 3(c) shows the evolution of the pre-exponential factor with the B/A ratio. In the epitaxial films, a small increase could be measured with an increase in the Mn content in the films. The pre-exponential factor is defined in the case of considering on-site Coulombic repulsions as[31,33]

$$\sigma_0 = \frac{e^2 \nu}{a k_b} \cdot \left[Mn^{4+}\right] \cdot \left[Mn^{3+}\right], \qquad (2)$$

where e, ν, and a are the electron charge, the polaron attempt frequency, and the site to site hopping distance, respectively. In the grain bulk, since negligible manganese valence changes were measured, the pre-exponential directly increases with the Mn content, $\sigma_0 \propto \left[Mn^{4+}\right] \cdot \left[Mn^{3+}\right] \propto [Mn]^2$. Thus, a decrease in the Mn concentration generates fewer sites for the polarons to hop, resulting in lower values of conductivity. As a matter of fact, the pre-exponential factor of the epitaxial LSM_y films perfectly follows this theoretical trend [blue dashed line in Fig. 3(c)], reinforcing the proposed defect model for the bulk material. Even more interestingly, polycrystalline films present a surprising increment of σ_0 as a function of Mn (from GB_{def} to GB_{rich}) indicating the great impact of the cation non-stoichiometry at the GB level. While in the presence of GB_{def} the pre-exponential factor is slightly smaller than the bulk (straightforwardly related to the extra Mn depletion at the GB), in the films dominated by GB_{rich} the increase is much higher suggesting the creation of additional pathways for electronic conduction probably enabled by the generation of anti-site Mn_{La}^x at the interface level.[34] The complementary σ_0 and E_a measured for the polycrystalline thin films deposited on YSZ/Si and on sapphire suggest that the substrate does not influence the GB composition and, therefore, the electrical properties. All in all, a remarkable impact of the GBs on the high temperature electrical conduction of polycrystalline samples is clearly proved.

Complementary to Fig. 3(a), Fig. 4(a) shows a representation of the conductivity of specific compositions of epitaxial and polycrystalline thin films according to the NNH conduction model, for the whole range of temperatures measured, namely, from 83 K to 873 K. According to this figure, nearly stoichiometric (B/A = 1.03) polycrystalline layers, as well as epitaxial thin films (both Mn-deficient, B/A = 0.85, and slightly Mn-rich, B/A = 1.05), present the typical metal-insulator (M-I) transition observed for LSM.[35] The less marked metallic behavior of the epitaxial Mn deficient epitaxial sample can be explained by the presence of scattered Mn vacancies, which are known to hinder the long range electronic order in manganites.[36–38] Opposed to that, a suppression of the M-I transition, maintaining the insulating
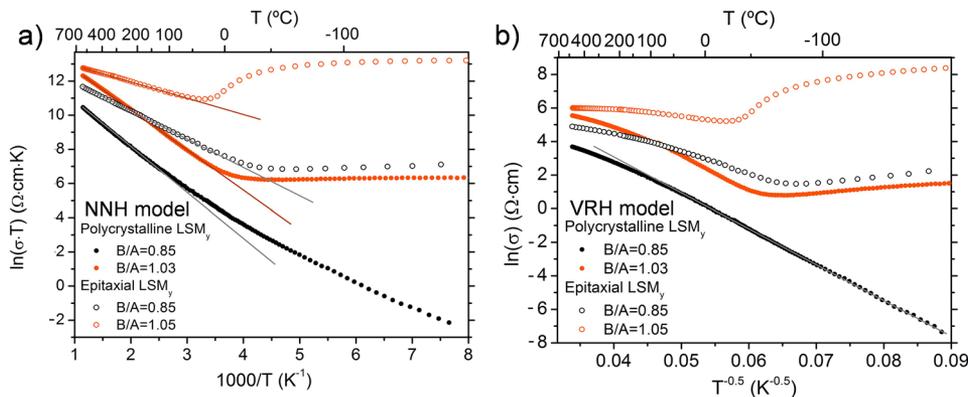
FIG. 4. In plane electronic conductivity plotted according to the adiabatic small polaron model (a) and to the SE-VRH model (b) for a wide set of temperatures. In the polycrystalline sample with B/A = 0.85, the first well describes the conductivity for T > 473 K, while for T < 473 K the second shows a better fitting.

behavior, is observed for the polycrystalline Mn deficient LSM_y; for further details, see Ref. 11. Moreover, its conductivity deviates from the linear behavior expected for the NNH model, approaching the typical performance of a Variable Range Hopping (VRH) conduction mechanism, Fig. 4(b), in which the probability of finding an available site with a proper energy level decreases with temperature, determining a temperature-dependent hopping length.[39] VRH theory was first developed for disordered materials and follows the general expression,

$$\sigma(T) = \sigma_p \cdot \exp\left(-\frac{T_0}{T}\right)^p, \qquad (3)$$

with T_0 being the characteristic temperature and p being the exponential term, which equals to $\frac{1}{4}$ in the case of a Mott regime[39] and $\frac{1}{2}$ for a Shklovskii–Efros (SE-VRH) mechanism.[40] For Mn-deficient polycrystalline LSM films, we found a good consistency with the SE-VRH model [see Fig. 4(b) and more details in Sec. S.6. of the supplementary material]. The appearance of VRH conduction in the polycrystalline films with GB_{def} is not intrinsic, but due to the localized defects in the GBs, the epitaxial film with the same composition shows a better agreement with the NNH adiabatic model in the whole temperature range above the occurrence of the M-I transition. Indeed, the onset of this mechanism was also previously reported in polycrystalline manganite thin films,[9,10] as well as in disordered bulk manganites[41,42] and ultrathin epitaxial thin films.[43] From the mechanistic point of view, the Mn deficiency and the presence of oxygen vacancies at the interface in GB_{def} of polycrystalline LSM_y films naturally hinder the insulator metallic behavior, giving rise to the VRH mechanism, in which polarons need to jump toward distant sites across the GB. The appearance of the SE-VRH could indicate that the charged defects in the GBs promote polaron trapping or that the density of states at the Fermi level is not constant (see Sec. S.6. of the supplementary material for additional details on the ES-VRH model).[41,42,44] The recovery of the M-I transition for GB_{rich} films indicates that the depletion of La is not playing an active role in the electronic conduction and that the oxygen defect equilibrium of these GBs is similar to the one of the bulk.

At this stage, it is clear that GBs in LSM_y films are in the origin of significant changes in the electrical properties of the films (E_a, σ_0 and suppression of M-I transition) and that a distinct conduction mechanism takes place, presumably linked to the previously reported local stoichiometric changes.[11] These most likely modify the defect chemistry of the bulk material (Mn deficient or not). In order to get deeper insights into the defect chemistry of LSM_y grain boundaries, we analyzed the high temperature oxygen partial pressure (pO_2) dependence of the in-plane electronic conductivity. The experiments were performed in a ProboStat test station (NorECs). The pO_2 in the station was controlled with a ZIROX oxygen pump and monitored with an oxygen lambda-sensor placed next to the sample. The temperature was set to 923 K for ensuring a fast equilibration with the atmosphere while preventing grain growth in the polycrystalline films.

Figure 5(a) shows the pO_2 dependence of the electrical conductivity for polycrystalline thin films with different compositions. The conductivities were normalized to the value measured at 50 ppm of oxygen to better visualize the relative changes originated by pO_2 since the Mn deficient samples show a much lower conductivity with respect to the stoichiometric ones (see Fig. S7 of the supplementary material). Results obtained for an epitaxial film with nominal composition B/A = 0.85 are also included for comparison. Interestingly, the Mn-deficient epitaxial sample displays the typical p-type behavior expected for the bulk defect chemistry, while for the polycrystalline samples, p-type and n-type like dependences are observed for B/A > 0.9 (GB_{rich}) and B/A < 0.9 (GB_{def}), respectively. Oxidation-reduction studies of the Mn-deficient polycrystalline samples shown in Fig. 5(b) prove the reversibility of the unusual n-type like response, discarding any type of stabilization issues and confirming that the phenomenon is directly linked to the high concentration of GBs present in the films. Moreover, complementary measurements on thicker samples with lower GB density (double grain size) corroborate the dominant role of the interfaces in the conductivity (Fig. S8 of the supplementary material) since two contributions could be clearly differentiated when changing pO_2, namely, a fast one with the unusual n-type like behavior attributable to GB_{def}
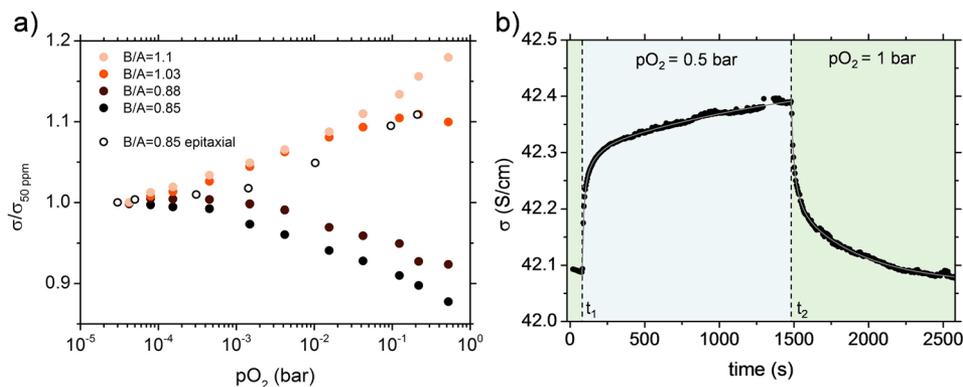
FIG. 5. (a) Relative in-plane electronic conductivity of the polycrystalline LSM_y films as a function of pO_2 [vs. the low pO_2 (50 ppm) conductivity] measured at 923 K. The epitaxial film with B/A = 0.85 is also reported for comparison. (b) Time response of the conductivity for reduction and oxidation steps at 923 K in the polycrystalline thin films with B/A = 0.85. The lines indicate the times at which the oxygen content in the atmosphere was changed (t_1 and t_2).

and a slower one showing the expected p-type conduction of the grain bulk.

As previously mentioned, the conductivity of GB_{rich} films follows the bulk behavior of LSM suggesting similar defect chemistry, i.e., incorporating oxygen by the creation of V'''_{Mn} and/or V'''_{La} combined with an increase of $[Mn^{4+}]$ that compensates the negative charges, resulting in the slight p-type oxygen dependence of the electronic conductivity.[45] On the contrary, the origin of the unusual pO$_2$ dependence of GB_{def} films is somehow more controversial. First, it could be due to the appearance of Mn^{2+} in the GB core, which would give rise to an n-type conduction even in oxidizing conditions.[21] However, our previous studies contradict this hypothesis since we did not observe any local change of oxidation state in GB_{def}.[11] Another possibility would be the creation of a negative space charge layer caused by the positive oxygen vacancies in the GB core, which could originate enrichment of negative elements (Mn^{2+}) in the GB surroundings.[46] Additionally, the presence of negative cation defects, which are also actively involved in the oxidation mechanism, could also play a role in defining the space charge properties.[47] Nevertheless, due to the high carrier concentration of the bulk and the small bandgap of LSM, the expected width of the space charge layer is extremely small, apparently ruling out this possibility.[7,48] Finally, a mechanism based on trapping positive charge carriers created upon oxygen oxidation may explain the pO$_2$ trend observed. Indeed, an increase of Mn^{4+} necessarily implies a decrease of Mn^{3+} and, according to Eq. (2), this could originate a decrease in the total conductivity (if Mn^{4+} is trapped). In any case, the appearance of this unusual pO$_2$ behavior is undoubtedly related to the characteristic depletion of Mn in GB_{def} and could have direct implications especially on the electrochemical performance of the layers and their stability in redox conditions. In this sense, we previously observed an outstanding stability of Mn deficient polycrystalline LSM layers when employed in symmetrical cells resulting in an anomalous weak dependence with pO$_2$ of their oxygen diffusivity,[49] contrary to what is expected from the defect chemistry models.[21]

In summary, we were able to fabricate high quality epitaxial and dense polycrystalline thin films of La$_{0.8}$Sr$_{0.2}$Mn$_{1-y}$O$_{3\pm\delta}$ with the B/A ratio ranging from 0.85 (Mn deficient films) to 1.2 (La deficient films). Conductivity measurements of epitaxial and polycrystalline LSM$_y$ thin films allowed us to elucidate the unique features of the GBs. From our study, it is clear that the electronic conductivity of the polycrystalline samples is dominated by the GBs, which largely impact the activation energy, the pre-exponential factor, and even the conduction mechanism at low temperatures. The origin of these effects is ascribed to the local non-stoichiometry at the GB level reported by our group in a previous study. Moreover, an unusual pO$_2$ dependency of the conductivity was observed as a function of the Mn content, indicating that different defect chemistries are required to fully describe the GB oxygen incorporation in LSM$_y$ films with different B/A ratios. All in all, the results of this work, combined with the recently discovered fast ion conduction along LSM GBs, anticipate a

radical change in the understanding and implementation of complex oxides in a collection of thin film-based solid state devices, especially for energy and information applications.

See supplementary material for Figs. S1–S7 and Refs. 1–26.

REFERENCES

[1] A. M. Saranya, D. Pla, A. Morata, A. Cavallaro, J. Canales-Vázquez, J. A. Kilner, M. Burriel, and A. Tarancón, Adv. Energy Mater. **5**, 1500377 (2015).

[2] E. Navickas, T. M. Huber, Y. Chen, W. Hetaba, G. Holzlechner, G. Rupp, M. Stöger-Pollach, G. Friedbacher, H. Hutter, B. Yildiz, and J. Fleig, Phys. Chem. Chem. Phys. **17**, 7659 (2015).

[3] A. M. Saranya, A. Morata, D. Pla, M. Burriel, F. Chiabrera, I. Garbayo, A. Hornés, J. A. Kilner, and A. Tarancón, Chem. Mater. **30**, 5621 (2018).

[4] E. Navickas, Y. Chen, Q. Lu, W. Wallisch, T. M. Huber, J. Bernardi, M. Stöger-Pollach, G. Friedbacher, H. Hutter, B. Yildiz, and J. Fleig, ACS Nano **11**, 11475 (2017).

[5] A. Asamitsu, Y. Tomioka, H. Kuwahara, and Y. Tokura, Nature **388**, 50 (1997).

[6] A.-M. Haghiri-Gosnet and J.-P. Renard, J. Phys. D: Appl. Phys. **36**, R127 (2003).

[7] R. Gross, L. Alff, B. Büchner, B. H. Freitag, C. Höfener, J. Klein, Y. Lu, W. Mader, J. B. Philipp, M. S. R. Rao, P. Reutler, S. Ritter, S. Thienhaus, S. Uhlenbruck, and B. Wiedenhorst, J. Magn. Magn. Mater. **211**, 150 (2000).

[8] A. Gupta, G. Q. Gong, G. Xiao, P. R. Duncombe, P. Lecoeur, P. Trouilloud, Y. Y. Wang, V. P. Dravid, and J. Z. Sun, Phys. Rev. B **54**, R15629 (1996).

[9] R. Prasad, M. P. Singh, W. Prellier, P. K. Siwach, R. Rawat, A. Kaur, and H. K. Singh, Phys. Status Solidi B **246**, 1662 (2009).

[10] M. Ziese and C. Srinitiwarawong, Phys. Rev. B **58**, 11519 (1998).

[11] F. Chiabrera, I. Garbayo, L. López-Conesa, G. Martín, A. Ruiz-Caridad, M. Walls, L. Ruiz-González, A. Kordatos, M. Núñez, A. Morata, S. Estradé, A. Chroneos, F. Peiró, and A. Tarancón, "Engineering transport in manganites by tuning local nonstoichiometry in grain boundaries," Adv. Mater. (published online).

[12] H. M. Christen, I. Ohkubo, C. M. Rouleau, G. E. Jellison, A. A. Puretzky, D. B. Geohegan, and D. H. Lowndes, Meas. Sci. Technol. **16**, 21 (2005).

[13] J. C. H. Rossiny, J. Julis, S. Fearn, J. A. Kilner, Y. Zhang, L. Chen, S. Yang, and J. R. G. Evans, Solid State Ionics **179**, 1085 (2008).

[14] J. A. Greer, J. Phys. D: Appl. Phys. **47**, 034005 (2014).

[15] H. M. Christen and G. Eres, J. Phys.: Condens. Matter **20**, 264005 (2008).

[16] A. H. De Vries, L. Hozoi, and R. Broer, Int. J. Quantum Chem. **91**, 57 (2002).

[17] J. García, G. Subías, V. Cuartero, and J. Herrero-Martin, J. Synchrotron Radiat. **17**, 386 (2010).

[18] G. Subías, J. García, M. Proietti, and J. Blasco, Phys. Rev. B: Condens. Matter Mater. Phys. **56**, 8183 (1997).

[19] V. R. Mastelaro, D. P. F. De Souza, and R. A. Mesquita, X-Ray Spectrom. **31**, 154 (2002).

[20] I. Maurin, P. Barboux, Y. Lassailly, J. Boilot, and F. Villain, J. Magn. Magn. Mater. **211**, 139 (2000).

[21] F. Poulsen, Solid State Ionics **129**, 145 (2000).

[22] M. Pavone, A. B. Muñoz-García, A. M. Ritzmann, and E. A. Carter, J. Phys. Chem. C **118**, 13346 (2014).

[23] K. Nakamura, J. Solid State Chem. **173**, 299 (2003).

[24] L. Qiao, K. H. L. Zhang, M. E. Bowden, T. Varga, V. Shutthanandan, R. Colby, Y. Du, B. Kabius, P. V. Sushko, M. D. Biegalski, and S. A. Chambers, Adv. Funct. Mater. **23**, 2953 (2013).

[25] D. Varshney and N. Dodiya, Mater. Chem. Phys. **129**, 896 (2011).

[26] A. Lanzara, N. L. Saini, M. Brunelli, F. Natali, A. Bianconi, P. G. Radaelli, and S.-W. Cheong, Phys. Rev. Lett. **81**, 878 (1998).

[27] M. Jaime, H. T. Hardner, M. B. Salamon, M. Rubinstein, P. Dorsey, and D. Emin, Phys. Rev. Lett. **78**, 951 (1997).

[28] D. Emin and T. Holstein, Ann. Phys. **53**, 439 (1969).

[29] F. Yang, S. Kim, and Y. Takamura, Scr. Mater. **65**, 29 (2011).

[30] C. Adamo, X. Ke, H. Q. Wang, H. L. Xin, T. Heeg, M. E. Hawley, W. Zander, J. Schubert, P. Schiffer, D. A. Muller, L. Maritato, and D. G. Schlom, Appl. Phys. Lett. **95**, 112504 (2009).

[31] J. Mizusaki, Y. Yonemura, H. Kamata, K. Ohyama, N. Mori, H. Takai, H. Tagawa, M. Dokiya, K. Naraya, T. Sasamoto, H. Inaba, and T. Hashimoto, Solid State Ionics **132**, 167 (2000).

[32] S. Mildner, J. Hoffmann, P. E. Blöchl, S. Techert, and C. Jooss, Phys. Rev. B **92**, 035145 (2015).

[33] D. C. Worledge, L. Mie, and T. H. Geballe, Phys. Rev. B **57**, 15267 (1998).

[34] C. Aruta, M. Minola, A. Galdi, R. Ciancio, A. Y. Petrov, N. B. Brookes, G. Ghiringhelli, L. Maritato, and P. Orgiani, Phys. Rev. B: Condens. Matter Mater. Phys. **86**, 115132 (2012).

[35] A. Urushibara, Y. Moritomo, T. Arima, A. Asamitsu, G. Kido, and Y. Tokura, Phys. Rev. B **51**, 14103 (1995).

[36] I. Marozau, P. T. Das, M. Döbeli, J. G. Storey, M. A. Uribe-Laverde, S. Das, C. Wang, M. Rössle, and C. Bernhard, Phys. Rev. B **89**, 174422 (2014).

[37] J. Vergara and V. Madurga, Phys. Rev. B **60**, 1127 (1999).

[38] S. Hébert, B. Wang, A. Maignan, C. Martin, R. Retoux, and B. Raveau, Solid State Commun. **123**, 311 (2002).

[39] N. F. Mott and E. A. Davis, *Electronic Processes in Non-Crystalline Materials* (Oxford University Press, 1971).

[40] A. L. Efros and B. I. Shklovskii, J. Phys. C: Solid State Phys. **8**, L49 (1975).

[41] R. Laiho, K. G. Lisunov, E. Lähderanta, P. A. Petrenko, J. Salminen, M. A. Shakhov, M. O. Safontchik, V. S. Stamov, M. V Shubnikov, and V. S. Zakhvalinskii, J. Phys.: Condens. Matter **14**, 8043 (2002).

[42] R. Laiho, K. G. Lisunov, E. Lähderanta, V. N. Stamov, and V. S. Zakhvalinskii, J. Phys.: Condens. Matter **13**, 1233 (2001).

[43] Y. Feng, K. Jin, L. Gu, X. He, C. Ge, Q. Zhang, M. He, Q. Guo, Q. Wan, M. He, H. Lu, and G. Yang, Sci. Rep. **6**, 22382 (2016).

[44] R. Laiho, K. G. Lisunov, E. Lähderanta, V. S. Stamov, V. S. Zakhvalinskii, P. Colomban, P. A. Petrenko, and Y. P. Stepanov, J. Phys.: Condens. Matter **17**, 105 (2005).

[45] L. Yan, K. R. Balasubramaniam, S. Wang, H. Du, and P. A. Salvador, Solid State Ionics **194**, 9 (2011).

[46] F. Chiabrera, I. Garbayo, and A. Tarancón, *Metal Oxide-Based Thin Film Structures* (Elsevier, 2018), pp. 409–439.

[47] W. Preis and W. Sitte, Solid State Ionics **177**, 2549 (2006).

[48] J. M. Polfus, B. Yildiz, and H. L. Tuller, Phys. Chem. Chem. Phys. **20**, 19142 (2018).

[49] F. Chiabrera, A. Morata, M. Pacios, and A. Tarancón, Solid State Ionics **299**, 70 (2017).